Layer-by-Layer Assembled Antisense DNA Microsponge Particles for Efficient Delivery of Cancer Therapeutics

Young Hoon Roh,[†] Jong Bum Lee,[†,‡] Kevin E. Shopsowitz, Erik C. Dreaden, Stephen W. Morton, Zhiyong Poon, Jinkee Hong,[§] Inbar Yamin, Daniel K. Bonner, and Paula T. Hammond*

Department of Chemical Engneering and The Koch Institute for Integrative Cancer Research, Massachusetts Institute of Technology, Cambridge, Massachusetts 02139, United States. [†]Y. H. Roh and J. B. Lee contributed equally to this work. [‡]Present address: Department of Chemical Engineering, University of Seoul, Seoul, 130-743, South Korea. [§]Present address: School of Chemical Engineering & Material Science, Chung-Ang University, Seoul, 156-756, Republic of Korea.

ABSTRACT Antisense oligonucleotides can be employed as a potential approach to effectively treat cancer. However, the inherent instability and inefficient systemic delivery methods for antisense therapeutics remain major challenges to their clinical application. Here, we present a polymerized oligonucleotides (ODNs) that self-assemble during their formation through an enzymatic elongation method (rolling circle replication) to generate a composite nucleic acid/magnesium pyrophosphate sponge-like microstructure, or DNA microsponge, yielding high molecular weight nucleic acid product. In addition, this densely packed ODN microsponge structure can be further condensed to generate polyelectrolyte complexes with a favorable size for cellular uptake by displacing magnesium pyrophosphate crystals from the microsponge structure. Additional layers are applied to generate a blood-stable and multifunctional nanoparticle *via* the layer-by-layer (LbL) assembly technique. By taking advantage of DNA nanotechnology and LbL assembly, functionalized DNA nanostructures were utilized to provide extremely high numbers of repeated ODN copies for efficient antisense therapy. Moreover, we show that this formulation significantly improves nucleic acid drug/carrier stability during *in vivo* biodistribution. These polymeric ODN systems can be designed to serve as a potent means of delivering stable and large quantities of ODN therapeutics systemically for cancer treatment to tumor cells at significantly lower toxicity than traditional synthetic vectors, thus enabling a therapeutic window suitable for clinical translation.

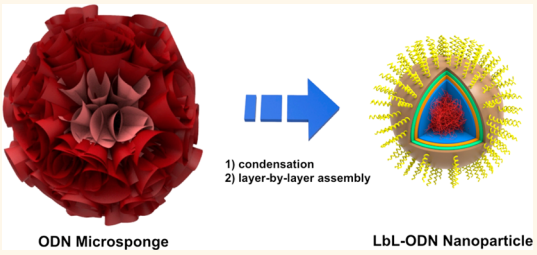

KEYWORDS: DNA nanotechnology · layer-by-layer · cancer · multifunctionality · antisense therapy · DNA oligonucleotide · DNA delivery

One of the major issues for the use of nucleic acids as active therapeutics for a broad range of cancers, infectious disease and other disorders is the safe and successful targeted delivery to specific organs upon systemic administration. We have reported an approach to generating a polymeric form of small interfering RNA (siRNA) that are effectively self-assembled into RNAi microsponge structures that can provide dense concentrations of siRNA ultimately accessible within nanoparticles with orders of magnitude lower concentrations of potentially toxic polycation[1] and described the mechanism of self-assembly and structure of these microsponges.[2] Along with RNAi, similar delivery challenges exist for other important forms of short regulatory nucleic acids like antisense oligonucleotides (ODN), which have a DNA backbone, and we seek to adapt these methods accordingly. Furthermore, it is necessary to introduce further modification of the self-assembled particles derived from these microsponges to achieve systems with appropriate biodistribution and plasma half-life for meaningful delivery to targeted tissues.

Recently antisense therapy has been introduced as one of the promising treatment approaches for cancer because of its specific target selectivity in gene silencing, an improved understanding of molecular mechanisms in specific tumor types, and the recent identification of therapeutic

* Address correspondence to hammond@mit.edu.

Received for review May 12, 2014 and accepted September 8, 2014.

Published online September 08, 2014
10.1021/nn502596b

target genes that were traditionally recognized as "undruggable".[3−7] When binding takes place, the bound ODN/RNA hybrids serve as substrates for enzyme-activated degradation (*e.g.*, RNase H) or physical blockage, resulting in the inhibition of translation of their target sequences. Despite the powerful therapeutic potential of ODNs, improved physicochemical properties of ODN backbones (*e.g.*, specificity and stability), and efficient systemic delivery strategies are important prerequisites for its clinical application in cancer. Several useful chemical modifications of ODN backbones have been reported to achieve improved resistance to nuclease digestion and prolonged *in vivo* half-life.[8−11] In addition, for efficient antisense therapy to be clinically realized, major challenges must be addressed to achieve desirable therapeutic windows, such as ensuring lower toxicity from delivery agents and the use of lower quantities of packaging agents so as to provide high amounts of active ODN drug loading per carrier and improved stability in systemic circulation.[12,13] In addition, the uptake of nanocarriers *via* endocytic pathways, its intracellular trafficking and effective endosomal escape, and the safe release of ODN drugs from nanocarriers to functional targets in the cytoplasm and nucleus should also be considered.[14−18] In order to deliver ODN therapeutics into a specific target area, rational design of nanoparticles is required based on particle size, surface chemistry, composition, shape, chemical functionality, and mechanism of action.[19]

An important aspect of DNA nanotechnology is the ability to engage molecular recognition and intrinsically define structural features with nanometer precision,[20−23] which facilitates the employment of useful strategies to construct functionalized DNA nanostructures for their use in biomedical applications.[24,25] Recently, several types of self-assembled functional DNA nanostructures, composed of relatively short oligonucleotides have been engineered for sensing, bioimaging, and drug delivery.[26−30] In particular, rolling circle replication (RCR) has been introduced as a powerful method for nucleic acid synthesis.[31] This process of nucleic acid replication is particularly favorable for the production of long repeated strands of nucleic acids in a stable form and at low cost. We have used rolling circle transcription (RCT) to create self-assembled RNAi microsponge structures[1] and more recently, the development of DNA hydrogels by using rolling circle amplification (RCA) has been reported.[32] Both of these examples clearly demonstrate the power of RCR in nucleic acid nanotechnology. Key to our approach is the generation of concatenated or polymeric forms of nucleic acids that can be broken down in cells by a native intracellular enzyme, Dicer, to short oligonucleotide sequences relevant to gene silencing.

The resulting condensed polyplexes generated from the microsponges can be directly modified using the versatile approach of layer-by-layer (LbL) assembly,[33,34] for which key design parameters such as layer components, layer number, and layer order, make this platform a valuable option for tuning the properties in therapeutic nanoparticle delivery systems.[35−40] Delivery vehicles fabricated *via* LbL assembly can carry multiple functional components, precisely control the release of therapeutic drugs, and facilitate improved biodistribution of the drug-containing nanoparticle system. Various types of LbL nanoparticle delivery systems have been reported to facilitate cellular uptake, improve both drug and carrier pharmacokinetics, and enhance molecular targeting capability.[41−48]

RESULTS AND DISCUSSION

As illustrated in Figure 1, we have developed a concatenated DNA-based LbL-assembled nanoparticle delivery platform. Using RCA, we initially generated self-assembled composite DNA microsponge structures containing ODN's in the form of long single-stranded oligonucleotide (ssDNA) polymers that each contain several thousands of repeated ODN copies complementary to a selected target sequence for antisense therapy. The DNA microsponges were then structurally disrupted by adding cationic polymers and salts, which displace the magnesium pyrophosphate crystals[2] that make up the scaffold of the microsponge; this process leads to the formation of nanosized complexes. Using this approach, we employed a long polymeric ODN as the core region and applied additional outer-layer shells *via* LbL assembly. By rational design and selection of biomaterials, we incorporated multiple functional moieties in each layer compartment. In addition, these LbL assembled polymeric ODN structures demonstrated higher resistance to nuclease digestion, prolonged *in vivo* half-lives, and controlled release to overcome the inherent difficulties in their delivery.

Antisense DNA Microsponge Particles. To generate antisense particles that can self-assemble into organized microstructures, we first designed and prepared a linear ssDNA encoding complementary sequences of ODN (see Supporting Information, Table S1). As a proof of concept for biological function, we incorporated DNA sequences complementary to antiluciferase ODN. The linear ssDNA strand (91 bases) was then hybridized with a primer ssDNA (22 bases), which was partially complementary to both ends of the linear DNA, to form a circular DNA. The nick inside the circular DNA was connected by enzyme ligation with a T4 DNA ligase. Gel electrophoresis was performed to demonstrate the synthesis of circular DNA from the linear DNA structure (see Supporting Information, Figure S1). A distinct band shift between circular and linear DNA was observed, indicating the successful assembly of circular DNA. In the RCA process, this engineered circular DNA was used as a template for generating repeated

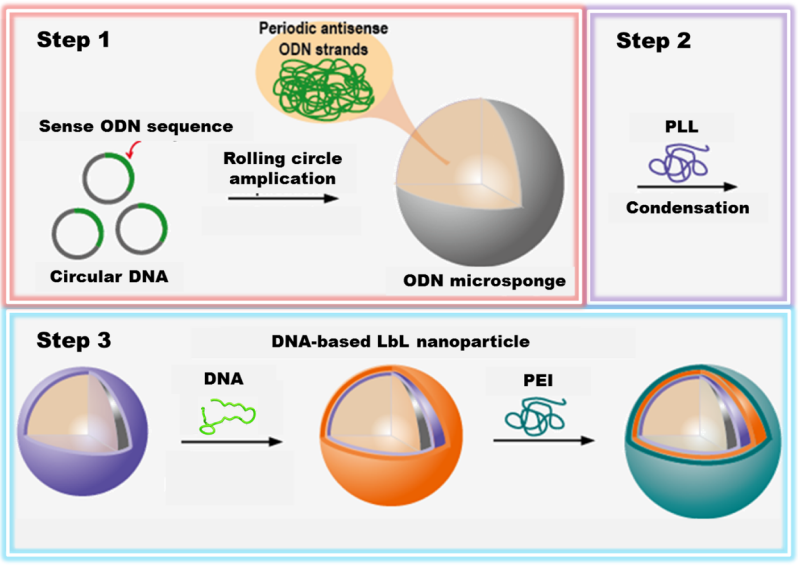

Figure 1. Design of the multifunctional DNA-based layer-by-layer assembled nanoparticle. Schematic illustration of the construction of multifunctional nanoparticle using three important strategies including the synthesis of antisense microsponge particles (ODN-MS), condensation process, and layer-by-layer assembly. A self-assembled microsponge-like structure of DNA containing a large amount of periodic antisense oligodeoxynucleotide (ODN) strand in the form of a long polymeric ssDNA was synthesized using rolling circle amplification (RCA) (Step 1). During condensation, ODN-MS were totally disrupted and then reconstructed into nanosized polyplexes by complexation with a selected polymer (Step 2). Next, keeping this complexation as the core, additional outer layer shells were formed through layer-by-layer (LbL) assembly technique (Step 3). Finally, these LbL-ODN nanoparticles (LbL-ODN-NPs) possessed multifunctionality due to the power of both functional DNA nanostructure and LbL assembly method.

polymeric ODN sequences. The reaction was carried out with high circular DNA concentrations (300 nM) in the presence of DNA polymerase and allowed to proceed for ~24 h at room temperature. Spherulitic sponge-like structures were formed consisting of a magnesium pyrophosphate crystalline phase that acts as a template for high loadings of polymeric ODN, for which each polymer strand contains approximately 1700 tandem repeats of antiluciferase ODN. To prepare more uniform particles, the reaction solution was sonicated until the products were well dispersed. The morphology and structure of the RCA product was further studied using various microscopy techniques. Scanning electron microscopy (SEM) images showed that the ODN composite microparticles were uniformly sized (~2 μm), exhibited sponge-like porosity, and were spheroidal in shape (Figure 2A,B). Because of their morphology and biological function, we refer to the resultant particles as oligodeoxynucleotide antisense microsponge particles (ODN-MS). In addition, transmission electron microscopy (TEM) images indicated that this structure was hierarchical, composed of multilayers of thin sheets that are further organized into a branched spherulitic structure. In the higher magnification TEM images, the two compartments are clearly visualized, including the multilayers of thin sheets and the highly branched structure inside the particle (Figure 2C,D). Because of the presence of magnesium pyrophosphate, the structure of the ODN-MS was readily visualized without metal staining, unlike typical DNA TEM imaging. Morphological characteristics of the ODN-MS were further analyzed using fluorescence and confocal microscopy to clearly visualize the distribution of DNA in the microsponges. In fluorescence microscopy analysis, the existence of ssDNA in these particles was indicated by staining with SYBR II, a DNA-specific dye, which exhibits green fluorescence only when it binds with ssDNA. On the basis of these observations, we confirmed that the generated DNA product existed in ssDNA form in the microsponge structure (see Supporting Information, Figure S2). Interestingly, a ring-shaped distribution of DNA was noticed in confocal microscopy images, indicating the highly localized presence of ssDNA at the edges of the particle surface. In this observation, we used both SYBR II staining after the microsponge structure formation and Cyanine 5-dUTP labeling during the RCA reaction, which results in bright red and green fluorescence, respectively (Figure 2E,F and Supporting Information, Figure S2).

We have demonstrated that ODN-MS consists of two different components. Here, one pyrophosphate anion (PPi) was produced from each nucleotide triphosphate during enzymatic nucleic acid polymerization by RCA. The resulting PPi product was bound by Mg^{2+} ions in the reaction buffer to form insoluble magnesium pyrophosphate (Mg_2PPi). To determine the structure of the ODN-MS, scanning transmission electron microscopy (STEM)-based energy dispersive X-ray spectroscopy (EDX) mapping was carried out to analyze the elemental composition of the ODN-MSs (Supporting Information, Figure S3). On the basis of

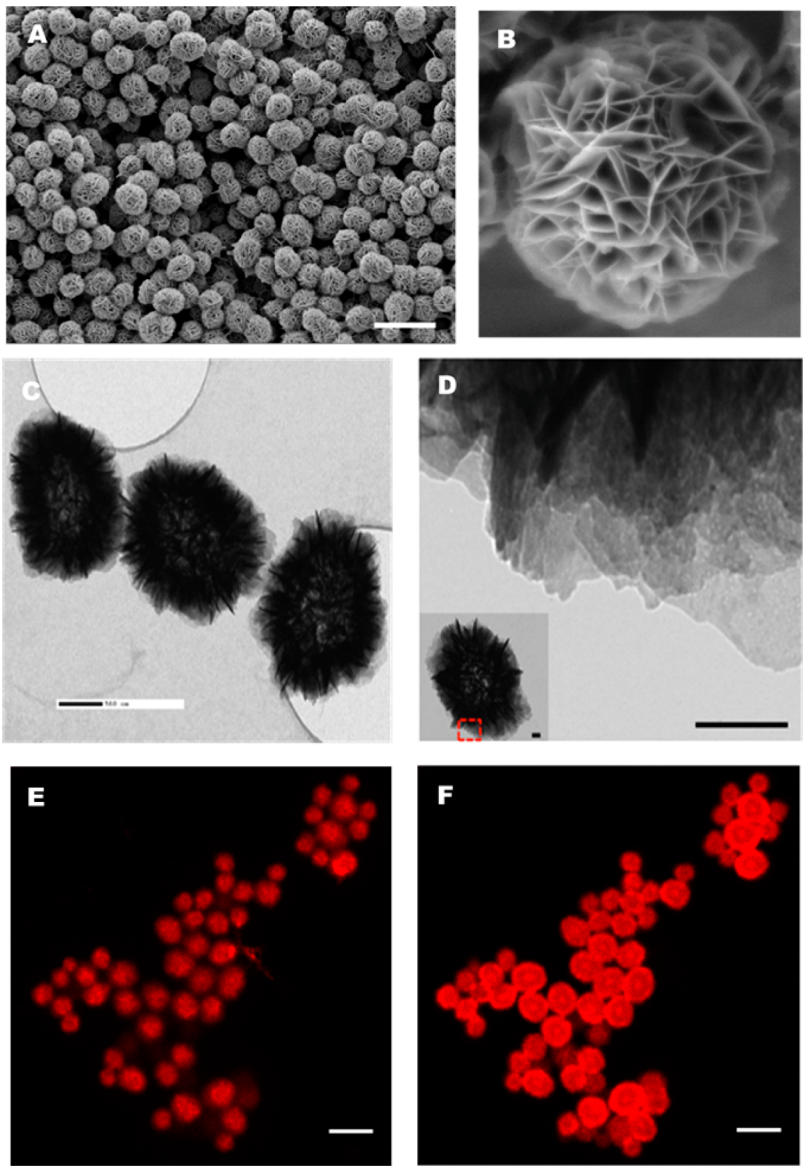

Figure 2. Structural characterization of antisense microsponge particle. (A,B) SEM images of ODN-MS. Scale bars indicate 5 μm (A) and 1 μm (B), respectively. (C,D) TEM images of ODN-MS observed at low and higher magnification. Scale bars indicate 500 nm (C) and 100 nm (D), respectively. (E,F) Confocal microscopy images of ODN-MS, which was functionalized with Cy5-conjugated dUTP during the RCA process (red color). ODN-MS viewed at top point (E) and in the middle section (F). Scale bars indicate 1 μm.

EDX, carbon (C) indicative of the presence of DNA, was found to be distributed in both the inner and outer particle regions. Similarly, magnesium (Mg), oxygen (O), and phosphorus (P) from $Mg_2P_2O_7$ were uniformly distributed throughout the particle. Point analysis of ODN-MSs using SEM-based EDX further supported the presence of carbon, oxygen, magnesium, and phosphorus, respectively, indicating a mixture of DNA and $Mg_2P_2O_7$ within the ODN-MSs (Supporting Information, Figure S4). To better understand the crystallization of ODN-MSs during RCA, we used powder X-ray diffraction (PXRD) to analyze their crystallinity (Supporting Information, Figure S5). The diffraction pattern matched well with the magnesium pyrophosphate phase $Mg_2P_2O_7 \cdot 3.5H_2O$. Taken together with the overall morphological and structural analysis of ODN-MSs, these supporting results suggest that the ODN-MSs generated during the RCA reaction are composed of DNA/inorganic composite materials, including densely packaged polymeric ODN and inorganic magnesium pyrophosphate crystals, similar to our observations for siRNA microsponges.[2]

We found that ODN strands from microsponges generated using the RCA approach were an unusually high molecular weight polymer structure. To confirm this notion, DNA microsponges were first prepared from circular DNA templates by RCA processes. These microsponges were then treated with EDTA to chelate Mg^{2+}. The subsequent DNA products were further analyzed using SEM and gel electrophoresis to

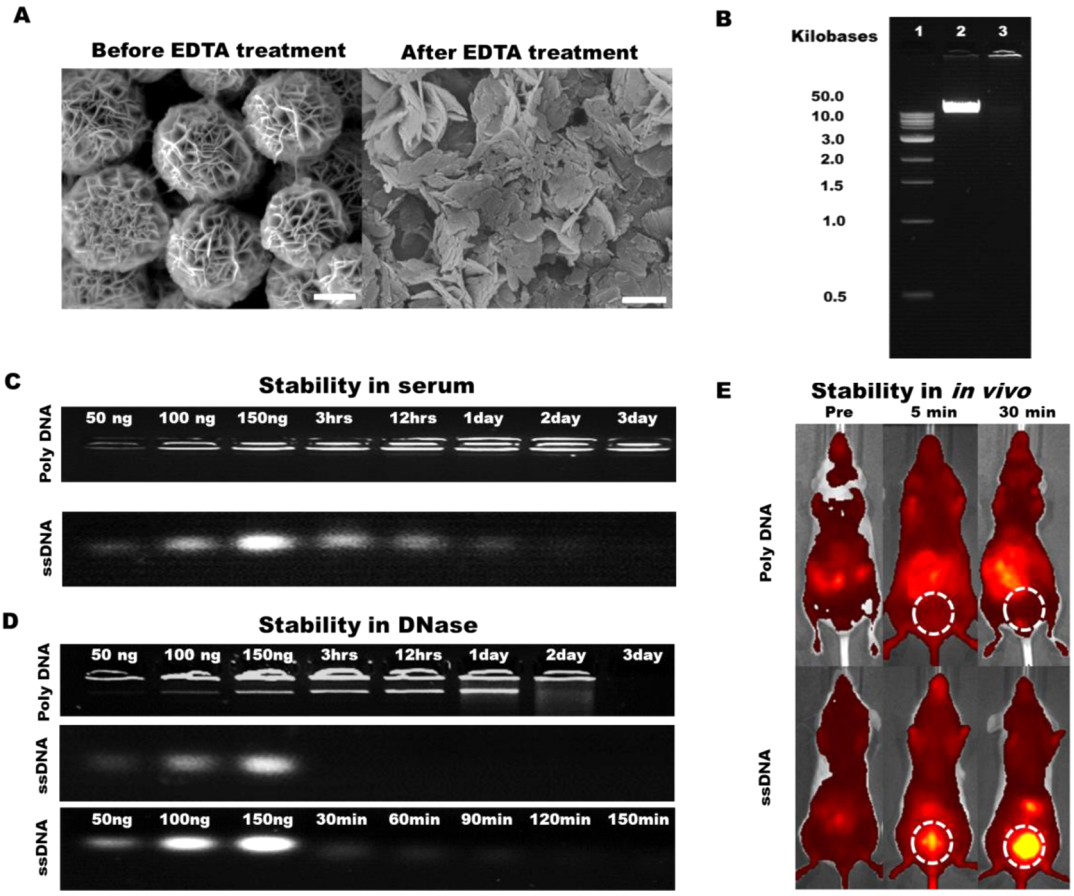

Figure 3. Characterization of polymeric DNA after extraction from antisense microsponge particle. (A) SEM images of ODN-MS before and after EDTA treatment. Scale bars indicate 500 nm. (B) Gel electrophoresis analysis to verify the size of polymeric DNA disrupted by EDTA. Lane 1−2 indicate 1 and 5 kb DNA ladder, respectively. (C) Serum stability of polymeric DNA (top) and short ssDNA (bottom) after a preassigned incubation time in a 50% serum medium. (D) Enzyme stability of polymeric DNA (top) and short ssDNA (bottom) after a preassigned incubation time in DNase (3 units/μL) at 37 °C. (E) *In vivo* stability of polymeric DNA and short ssDNA. Biodistribution of polymeric DNA (top) and short ssDNA (bottom) prior to injection followed by 5 and 30 min postinjection in NCr nude. Images are representative of a photograph with fluorescent overlay (λ_{ex} = 640 nm, λ_{em} = 700 nm).

characterize the polymeric size of DNA. SEM images indicated that the structure of ODN-MS was completely disrupted by the additional EDTA treatment (50 mM) facilitating the direct comparison of polymeric structures from particles (Figure 3A). Gel image showed that polymeric DNA was observed to run at a higher position on the gel indicating an extremely large product greater than 150 kb, corresponding to approximately 43 million Da (Figure 3B).[49] Here, we confirmed that the generated DNA structures from the microsponge system were very long polymeric structures, which correspond to the number of ODN repeating units. On the basis of the molecular weight analysis, several thousand (~1700) ODN repeats, each of which have the specifically programmed target function of the ODN sequence, could be generated during the RCA process and incorporated into the ODN-MSs. In order to further examine the size of the incorporated DNA polymer into microsponges during the DNA synthesis process, we conducted a time course study of polymerized DNA products during varied RCA reaction times. At each reaction time point, ODN-MSs were isolated and DNA polymer sizes were compared by gel electrophoresis after disruption of the particles by EDTA. On the basis of the results from gel electrophoresis, high molecular weight DNA polymers were rapidly generated and incorporated even in the initial stages of microsponge formation (roughly equivalent to the 8 h RCA reaction) (Supporting Information, Figure S6 and Lane 2, 4, 6); these sizes are significantly greater than those observed for the siRNA systems.[1,2] We performed a fluorescence-based measurement to quantify DNA loading in the ODN-MSs (see Supporting Information). DNA loading within the microsponge was approximately 12.5 ± 1.8 wt %; overall, we postulate that the localized loading of DNA at the edge of the particle may be due to the higher molecular weight of the ssDNA.

We demonstrated that the long chain polymeric ODN generated from the microsponge system exhibited dramatically improved serum and nuclease stability, presumably due to the protective effect of its

polymerized form. We used an ssDNA quantification assay and gel electrophoresis to confirm this finding by evaluating the stability of the isolated polymeric ODN structure from microsponge under the harsh conditions of high serum (50%) and DNase (3 units/μL) concentrations, respectively. Serum stability results indicated that the polymeric ODN structure showed a significantly improved intrinsic stability compared to a standard short ODN (~22 bases). The amount of short ODN decreased with increasing serum incubation time (50% loss within 3 h). However, the polymeric ODN structure was extremely well protected from serum treatment during the 3 days of incubation (Figure 3C and Supporting Information, Figure S5), and essentially maintained its large size. Furthermore, the treatment of short ODNs with DNase caused them to fully degrade, leaving them undetectable by gel electrophoresis (within ~15 min). In contrast, although some damage was observed under these harsh enzymatic conditions and long incubation times (3 days), the polymeric ODNs were significantly more resistant to DNase enzyme degradation (Figure 3D and Supporting Information, Figure S7). To further explore the systemic delivery of the polymeric ODN, we performed an *in vivo* pharmacokinetics study in NCr nude mice. Mice were injected *via* the tail vein with Cy5 dye-labeled polymeric or short ODNs and compared using whole-animal and blood fluorescence imaging to understand the biodistribution and blood half-life and stability of these systems. Rapid clearance for short ODN was observed, as evident by a significant bladder signal (circled, 73% injected dose, based on bladder radiant efficiency signal relative to the total integrated fluorescence recovered) present as early as 5 min, while comparatively no bladder signal was evident for the polymeric ODN up to 30 min, validating the avoidance of renal filtration by polymeric ODN due to size (Figure 3E). Overall, the isolated polymeric ODN from microsponges was significantly protected from serum and enzyme degradation, and reduced *in vivo* renal clearance.

Polymeric ODN Packaging by Condensation. For achieving desirable cellular and systemic ODN delivery efficiency, it is essential to obtain favorable sizes and appropriate surface properties with compact ODN structures. In our approach, the ODN-MS structures were disrupted and the DNA product encapsulated in an additional process (*i.e.*, a condensation step) to control morphology, charge, particle size, and surface structure. We further investigated the mechanism of this polymeric DNA packaging process during polycation condensation starting from the DNA/inorganic composite microsponge particles (ODN-MS). As we demonstrated previously, the microsponge can be easily broken down from its original structure by sequestering Mg^{2+} using chelating agents such as EDTA. In place of EDTA, we used cationic polymers (*e.g.*, poly-L-lysine: PLL) to act as a condensing agent for DNA. ODN-MS has a highly negative surface charge (-37.14 ± 1.46 mV) due to the presence of DNA and a relatively larger size (~1800 nm). The positively charged PLL binds readily with ODN-MS by electrostatic interactions, forming complex structures above a certain threshold concentration with the composite structure. Following this condensation step, ODN-MS transforms into a highly compact sized structure facilitating polymeric ODN drug loading. We realized that the major parameter required for this condensation process is the initial reaction concentration of the positively charged polymeric condensing agent in the presence of salts (Supporting Information, Table S2). To find out the optimal conditions for condensation, PLL concentration was varied from 0.1−5 mg/mL. The morphology of the condensed ODN-MS products was compared with initial ODN-MSs using various microscopic techniques. SEM images showed that ODN-MS microstructures change their morphology during condensation depending on the concentration of the polycation. At intermediate concentrations of PLL (1.5 mg/mL), the particles decreased in size (approximately 1 μm) and became less porous than the initial ODN-MS structure (Figure 4A,B); however, we observed the formation of nanosized complexes as the PLL concentration was increased (3 mg/mL, N/P = 0.5) (Figure 4C). We further examined the condensed structures by carrying out confocal microscopy with a dual-labeled fluorescence system (polymeric ODN: green color and PLL: red color) to observe the progression from microsponge to polyelectrolyte complexation. Confocal microscopy images were consistent with observations by SEM, which indicated that the initial microsponge structure decreased in size and formed condensed structures (Figure 4D−G). There was no change in the ODN-MSs at low PLL concentrations (below 0.4 mg/mL) in terms of the particle size and surface charge. PLL appears partially adsorbed to the ODN-MSs at intermediate concentrations of PLL (between 0.4−0.8 mg/mL). The shift of particle surface charge from -37.2 ± 1.5 mV (ODN-MS) to $+4.6 \pm 5.2$ mV (ODN-MS/PLL) after exposure to 0.8 mg/mL PLL concentration supports the presence of PLL in the particles (Figure 4H,I). Interestingly, at an intermediate concentration of PLL (1.5 mg/mL), we observed that the ODN-MSs shrunk from ~2 μm to approximately 1 μm, and that PLL was highly localized around the surface of ODN-MSs. This was indicated by a red hue (corresponding to PLL) that surrounds the green colored regions corresponding to polymeric ODN. At certain thresholds of PLL concentration (3 mg/mL), these structures form nanosized polyplex structures composed of both PLL and polymeric ODN molecules, which are observed as yellow in color (corresponding to a merged color from both polymeric ODN and PLL). At this PLL concentration, we observed successful polymeric ODN-loading into

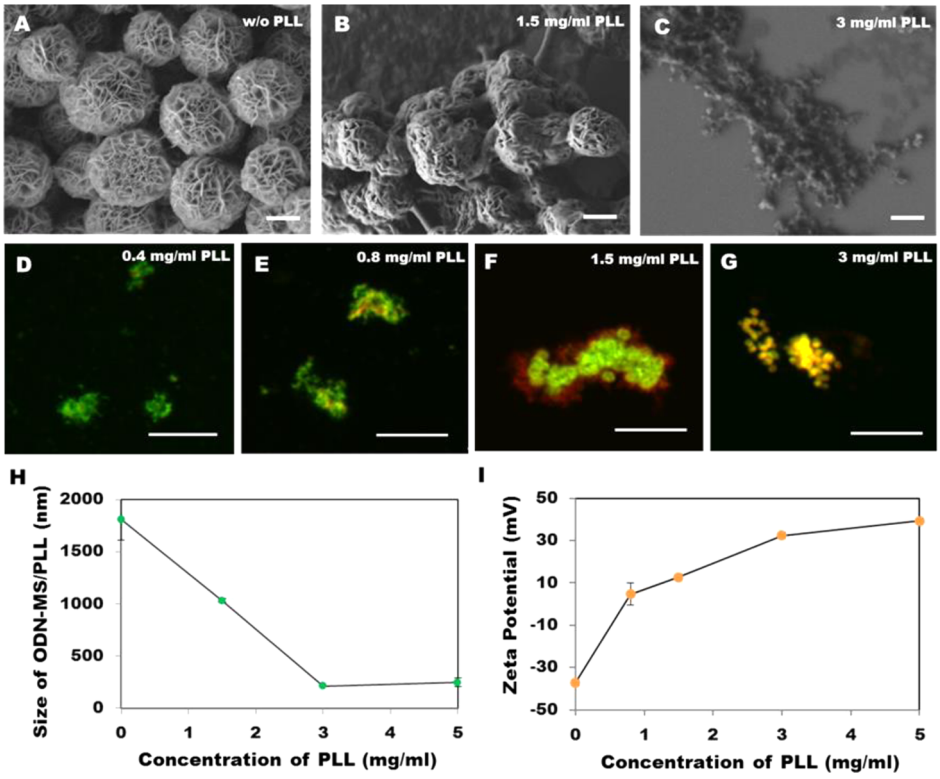

Figure 4. Characterization of polymeric DNA packaging by condensing process (A−C) SEM images of ODN-MS before condensing process (A) and after condensation with varying concentrations of PLL (B,C). Scale bars indicate 1 μm. SEM images show the reduced size of condensed nanoparticles with changed morphology. (D−G) Confocal microscopy images of ODN-MS after condensation with varying concentrations of PLL. Dual labeling was applied in this observation. PLL was functionalized with Cy5 (red color) and DNA was stained with SYBR II, ssDNA specific dyes (green color). Magnification was 60×, and scale bars indicate 5 μm. (H) Size of ODN-MS/PLL at varied concentrations of condensing polymer. (I) ζ Potential of ODN-MS/PLL at varying concentrations of condensing polymer.

polyplexes following the reconfiguration of the ODN-MSs. Following the condensation process, particles were isolated from free polycation in solution by dialysis. The ODN particles derived from the condensing process were further investigated by dynamic light scattering (DLS) and zeta (ζ)-potential analysis (Figure 4H,I). As shown in Figure 4H, the size of complex particles significantly decreased to 212.5 $\pm$ 15.6 nm after the condensing process. The average size of the original ODN-MSs was approximately 1800 $\pm$ 196.1 nm. ζ-potential also helped in the verification of the self-assembly of PLL with polymeric ODN. The change of particle surface charge from -37.2 ± 1.5 mV (ODN-MS) to $+32.4 \pm 1.6$ mV (ODN-MS/PLL) indicated the successful complexation of polymeric ODN with PLL (Figure 4I). Our results also suggest that the outer surfaces of the particle were saturated at 3 mg/mL of PLL solution because a significant increase in ζ-potential was not observed at higher concentrations of PLL. We performed elemental analysis for further investigation of the polymeric ODN packaging process using SEM-based EDX. Large differences between the relative amounts of O, Mg, and P were observed after condensation along with dramatically increased relative amounts of C and N, which suggests the successful release of magnesium pyrophosphate and the incorporation of polymer (PLL) during condensation (Supporting Information, Figure S4). Here O, Mg, and P represent the presence of magnesium pyrophosphate ($Mg_2P_2O_7 \cdot 3.5H_2O$). In addition, both C and N indicate the presence of the polymer-based condensing agent (*e.g.*, PLL). Further characterization of DNA packaging before and after condensation was carried out using powder XRD (PXRD). Specifically, the diffraction pattern of the ODN-MSs after condensation did not indicate the presence of magnesium pyrophosphate crystals in the particle (Supporting Information, Figure S5); instead we observed a large broad peak consistent with amorphous polymer. These results demonstrate that PLL is capable of triggering the release of magnesium pyrophosphate from the ODN-MSs during condensation with the DNA product.

Overall, we found that the ODN-MS rearranges to form smaller nanoparticle complexes at certain threshold concentrations of polycation during condensation. This was attributed to electrostatic interactions and physical agitation along with the release of magnesium pyrophosphate crystals. In conventional ODN complexation approaches with polymers or lipids, the amount of ODN per particle is very limited due to the low surface charge and relative rigidity of short ODNs, making their encapsulation especially challenging.

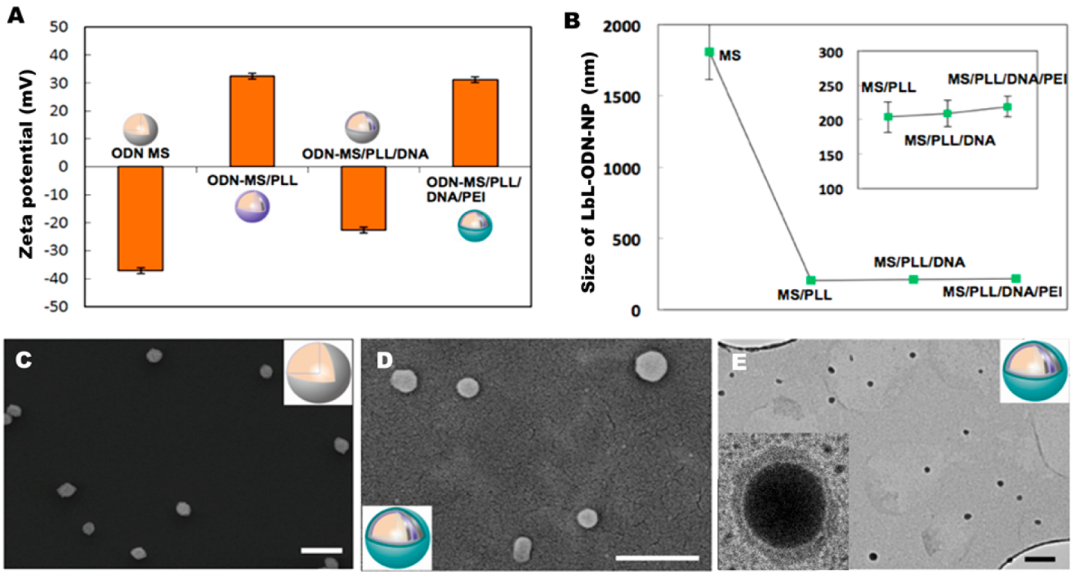

Figure 5. Properties of layer-by-layer assembled antisense microsponge particles. (A) ζ Potential of ODN-MS, ODN-MS/PLL, ODN-MS/PLL/DNA, and ODN-MS/PLL/DNA/PEI. (B) Size of ODN-MS, ODN-MS/PLL, ODN-MS/PLL/DNA, and ODN-MS/PLL/DNA/PEI. (C,D) SEM images of ODN-MS (C) and ODN-MS/PLL/DNA/PEI (D). Scale bars indicate 5 and 0.5 μm, respectively. (E) TEM image of ODN-MS/PLL/DNA/PEI. Scale bar indicates 1 μm.

In contrast, this approach uses a unique nucleic acid packaging process, generating highly stabilized and densely packed complexes due to the physicochemical properties of the structured microsponge such as a high localized surface charge density, and large surface area presenting localized concentrations of ODN with the improved condensation energetics and thermodynamic driving forces of polymeric ODN compared to rigid short ODN structures.[50] We believe that this process also allows a large amount of ODN encapsulation due to the localization of the negatively charged polymeric DNA on the microsponge surfaces, which facilitates polycation complexation of nucleic acids at higher concentrations relative to solution complexation.[51]

Properties of Layer-by-Layer Assembled Antisense DNA Microsponge Particles. By first layering with PLL to condense the polymeric antisense DNA, we can achieve a favorable size for cellular uptake, while maintaining a highly concentrated polymeric ODN nanoparticle core for enhanced drug delivery. Additional functional moieties can be incorporated onto these structures *via* LbL assembly to create an outer shell around the core, including the incorporation of polyions that provide the appropriate charge and hydration to achieve desirable biodistribution, and the introduction of targeting moieties. In order to use the power of DNA as a generic layering material in an LbL system, we used a short length of synthetic ssDNA (30 bases) for the second layer. Because of the high positive charge density of the PLL/ODN core nanoparticles, a negatively charged short ssDNA structure was readily adsorbed onto the particles through electrostatic interaction. The resulting DNA-layered PLL/ODN particle (referred to as ODN-MS/PLL/DNA) was then assembled again with linear polyethylenimine (PEI), which is an effective endosomal escape agent,[52] as the third layer (referred to as ODN-MS/PLL/DNA/PEI). The particle surface charge (ζ-potential) and hydrodynamic size (DLS) of LbL-ODN particles were characterized. The particle surface charge was inverted during each layering step, indicating that the additional layer was constructed in a stepwise fashion followed by alternating electrostatic interactions. Initially, the ODN-MSs were layered at 3 mg/mL PLL, resulting in a positive surface charge ($+32.4 \pm 1.6$ mV). These positively charged particles were used for *in vitro* studies in which the charge facilitates cell entry; whereas, *in vivo* experiments used a final neutral PEG outer layer for bloodstream stability and to create a stable stealth layer. The assembly of short ssDNA strands onto the PLL/ODN particle was successfully achieved by electrostatic adsorption, resulting in a shift in ζ-potential to -23.0 ± 1.4 mV (Figure 5A). Similarly, a positive ζ- potential from the ODN-MS/PLL/DNA/PEI verified PEI self-assembly onto the ODN-MS/PLL/DNA particles (Figure 5A). The size of the ODN-MS/PLL/DNA/PEI particles was 223 ± 8.6 nm in diameter following deposition of three layers onto the ODN-MSs (Figure 5B). On the basis of their sizes and structures, we termed these nanoscale and polymer-layered particles as LbL-ODN nanoparticles (LbL-ODN-NPs). These LbL-ODN-NPs were further examined using SEM and TEM. Images of ODN-MS/PLL/DNA/PEI also show well dispersed particles with a diameter of ~200 nm, which is compatible with the DLS results (Figure 5C–E). In comparison to earlier LbL-based DNA encapsulation papers[53,54] we find that (1) the ODN-MS system can incorporate a polymeric form of functional DNA (extremely large amounts of functional ODN unit

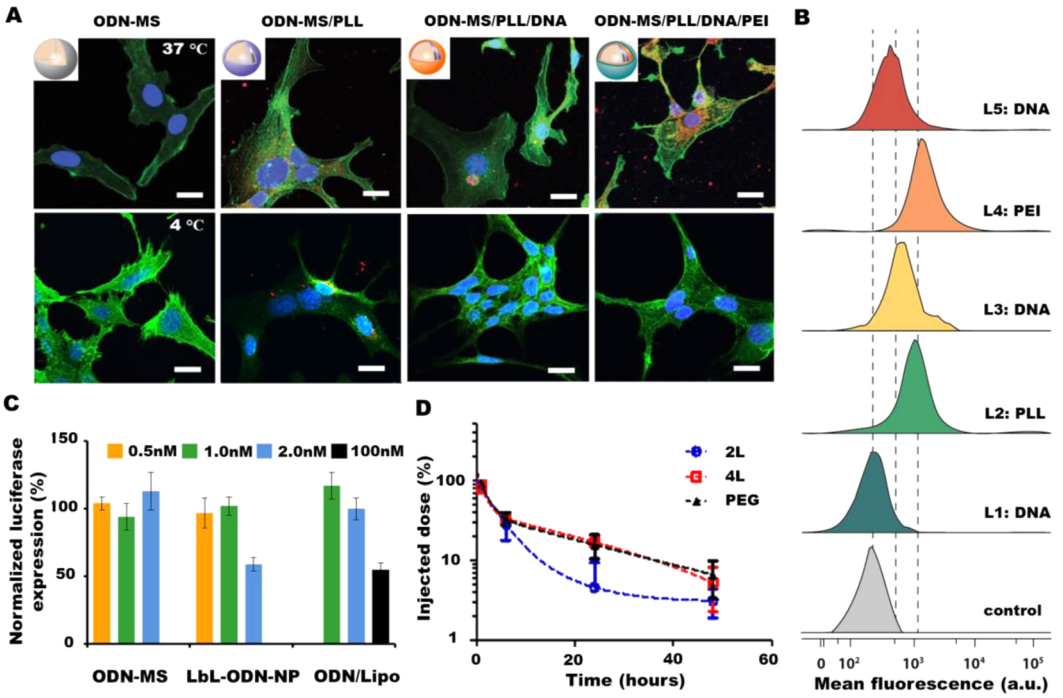

Figure 6. Intracellular and *in vivo* delivery of layer-by-layer assembled antisense DNA microsponge particles. (A) Intracellular delivery of layer-by-layer assembled antisense microsponge particles. Confocal microscopy image of cancer cells (*e.g.*, SKOV3) treated with LbL-ODN-NPs. Nanoparticles were labeled red with Cy5. The actin cytoskeleton was stained green with phalloidin, and the nucleus was stained blue with DAPI. Scale bars are 10 μm. (B) Cellular uptake study of LbL-ODN-NPs in cancer cells (*e.g.*, SKOV3) by using flow cytometry analysis. (C) The knockdown efficiency of target gene expression for firefly luciferase regulation using LbL-ODN-NPs was examined as a function of concentration *in vitro*. (D) Pharmacokinetics of nanoparticle clearance from IV-administered BALB/c mice with various LbL-ODN-NPs formulations fit with a 2-phase decay model (PRISM). ODN-MS/PLL/DNA (2L), ODN-MS/PLL/DNA/PEI/DNA (4L), ODN-MS/PLL/DNA/PEI/PEG (PEG).

per molecules) rather than just plasmid DNA, (2) improve therapeutic nucleic acid loading efficiencies, (3) can be adapted to undergo particle size changes from micro- to nanometer in scale during condensation for favorable biological applications (*e.g.*, drug delivery).

Intracellular and *In Vivo* Delivery of Layer-by-Layer Assembled Antisense DNA Microsponge Particles. In the next step, we analyzed the biological functions of LbL-ODN-NPs in terms of intracellular delivery and polymeric ODN drug delivery efficiency. To evaluate the genetic function of polymeric ODN, we performed *in vitro* investigation of the cellular uptake, knockdown efficiency, and cell viability. In order to investigate the efficacy of polymeric ODN delivery *in vitro*, we prepared various types of Cy5-labeled LbL-ODN-NPs by varying multilayer number and corresponding surface charge. The synthesized nanoparticles were transfected into cancer cells (*e.g.*, SKOV3) to observe the extent of cellular uptake. Confocal microscopy results indicated that LbL-ODN-NPs were successfully delivered into the cells (3 h, complete medium) (Figure 6A). Moreover, cellular uptake of ODN-MS/PLL/DNA/PEI particles in SKOV3 cells was qualitatively greater than that of the uncondensed ODN-MS, suggesting that their larger size and net negative surface charge inhibits efficient transfection. Cellular uptake of ODN-MS/PLL/DNA/PEI particles was attributed to ATP-mediated endocytosis because very low fluorescence signal was observed within the cells following incubation at 4 °C. We further investigated the cellular uptake of LbL-ODN-NPs by measuring fluorescence intensity of dye-labeled particles using flow cytometry (FACS) (Figure 6B). Similar trends in cellular uptake were observed from FACS, validating the confocal microscopy observations. Particles with a positively charged outer surface layer (both ODN-MS/PLL/DNA/PEI and ODN-MS/PLL) exhibited greater cellular uptake, as anticipated, due to charge interactions and nonspecific cell uptake. Moreover, these architectures formed stable structures after four successive layers (ODN-MS/PLL/DNA/PEI) and exhibited significant uptake because of the intrinsic polycationic properties of PEI (Supporting Information, Figure S8). These results suggest that employment of appropriate layer numbers and selection of biomaterials play a key role in LbL-ODN-NP cellular delivery. We also performed *in vitro* gene knockdown to examine the therapeutic efficiency of LbL-ODN-NPs (*e.g.*, ODN-MS/PLL/DNA/PEI). As a proof of concept, we chose firefly luciferase as a genetic target of interest. Measurement of the luciferase intensity after transfection indicated a substantial inhibition of gene expression (45.7 $\pm$ 6.8%) due to the silencing effect of polymeric ODN from ODN-MS/PLL/DNA/PEI (Figure 6C). Compared to conventional lipid-based transfection strategies (*e.g.*, lipofectamine),

knockdown from polymeric ODN showed ~50 fold improved efficiency relative to knockdown from ODN with lipofectamine in terms of the ODN concentration from ODN-treated cells. Cell viability after treatment with ODN-MS/PLL/DNA/PEI was also measured by the MTT assay, indicating low toxicity particles (Supporting Information, Figure S9). We expect that polymeric ODN delivery after LbL assembly will result in improved therapy due to augmented nuclease stability, high drug loading, efficient delivery, and low cytotoxicity.

Because of the rapid clearance of short ODN with a short plasma half-life *in vivo* (less than ~5 min), it is highly important to establish improved *in vivo* stability of ODN. Assessment of LbL as a means to stabilize ODN was performed by fluorescent modification of the polycationic component (PLL) of the film with a near-infrared dye (Cy5.5) to generate dye-labeled LbL-ODN-NPs, specifically ODN-MS/PLL-Cy5.5/DNA (2L) and ODN-MS/PLL-Cy5.5/DNA/PEI/DNA (4L) nanoparticles were constructed to examine the biodistribution of particles with net negative charge based on the non-specific synthetic DNA outer layer. For a more general outer stealth layer using a well-reported neutral protective hydrophilic polymer in circulation, polyethylene glycol (PEG)[55] was also incorporated in the final layer of LbL-ODN-NPs using a block copolymer with a negative charged polymer and PEG (*e.g.*, PEG-*b*-poly-L-glutamic acid), referred to ODN-MS/PLL/DNA/PEI/PEG (PEG). The biological performance of these systems was compared in immune-proficient BALB/c mice by whole-animal fluorescence imaging up to 48 h after IV injection. As shown in Figure 3E, the structure of the ODN alone was not suitable for *in vivo* drug delivery due to the rapid clearance of this therapeutic. The ODN-MS/PLL/DNA/PEI/DNA (4L) showed improved biological performance relative to nanoparticles with ODN-MS/PLL/DNA (2L) (Figure 6D and Supporting Information, Figure S10). The ODN-MS/PLL/DNA/PEI/PEG (PEG) nanoparticles also showed longer blood circulation persistence with additional layering and steric stabilization by PEG. Both the 4L and PEG constructs from this study were observed to be good packaging systems for the polymeric ODN construct. The results from *in vivo* fluorescence recovery from live-animal bleeds for blood circulation determination were further substantiated by tissue necropsy (Supporting Information, Figure S10). Reduced renal clearance was also observed with additional outer layers (4L and PEG) implying the protective effect of the polymeric ODN molecule cores due to the presence of additional layers for extended circulation profiles. Moreover these LbL-ODN-NPs showed a significantly prolonged and a broad range of controlled plasma half-life in comparison to the currently used chemically modified ODNs (*e.g.*, the phosphorothioate (PS) linkages in ODNs and the 2′-*O*-methoxyethyl (MOE) modified ODNs: less than 2−4 h compared to the LbL-ODN-NPs 19−25 h.[3,56] In addition different biodistribution tendencies were obtained when compared to the layered particles (Supporting Information, Figure S10). We monitored the accumulation of the engineered LbL-ODN-NPs in five major organs by *ex vivo* fluorescence images at 24 h postinjection. The kidney and liver were the primary organs of LbL-ODN-NPs accumulation, however these compounds were also distributed widely throughout the body. A certain level of quantified fluorescence signal from liver (~22% ID/g) was also detected within 24 h after LbL-ODN-NPs systemic injection. This system compares similarly to other reported nanoparticle systems with regard to biodistribution and liver accumulation, including LbL particles[43,45] and pegylated liposome.[57] Furthermore, we emphasize that the DNA-based LbL-assembled nanoparticle system (*e.g.*, ODN-MS/PLL/DNA/PEI/DNA) can be used in systemic delivery applications because of its improved stability for longer periods of time *in vivo*. Taken together, these improved biological performances were attributed to the selection of appropriate biomaterial candidates for tuning the surface properties of the ODN nanoparticles, the stability of inherent polymeric ODN, and the use of stabilizing LbL architectures. Further modification of the outer layers can be achieved for specific tumor types using targeting moieties, as we have shown with other LbL nanoparticle systems.[43,45,58,59]

CONCLUSIONS

Our work on DNA-based LbL-ODN nanoparticle systems is unique in terms of the use of polymeric DNA as a therapeutic agent, LbL assembly, and functionalization. This study successfully demonstrates the synthesis of DNA-based microsponge particles that contain highly concentrated polymeric nucleic acids (*e.g.*, ODN) and magnesium pyrophosphate crystals. Furthermore, this report demonstrates specific condensation processes to package large amounts of polymeric ODN within a nanoparticle core. Unlike conventional ODN-loading process with lipids and polymers, ODN-MSs require an additional procedure to disrupt their inorganic structure and reassemble into nanosized polycation complexes. This approach allows the encapsulation of polymeric DNA-based molecules such as ODN for therapeutic purposes for efficient drug loading and delivery. Moreover, by employing LbL assembly onto the condensed ODN-MSs, fine-tuning of their multifunctional properties can be achieved for imaging, and tunable surface charge, resulting in an improved intracellular uptake and therapeutic efficacy with a negligible cytotoxicity. This platform possesses multifunctionality because of the selection of appropriate biomaterials, which include PLL, DNA, PEI, and PEG. In addition, this electrostatically assembled multilayered nucleic acid delivery system provides enhanced pharmacokinetic stability by manipulating

surface chemistry and the number of particle layers, allowing for efficient systemic delivery. Because the layering of LbL-ODN-NPs system can be modularly and precisely controlled, further modification of the particles multifunctionality is possible for other applications by rationally combining biofunctional polyelectrolytes along with DNA. Our group is extensively investigating further systemic applications in cancer therapy and their efficacy toward specific diseases and tumor targets. This DNA-based modular platform approach offers the promise of a potent delivery method for nucleic acid therapeutics for cancer treatment.

METHODS

Circular DNA Template Design. The circularized ssDNA was used as a template for RCA. To prepare oligonucleotide sequences, linear ssDNA (91 bases) was designed to be comprised of a sequence complementary to the antisense sequence (red color in Figure S1, Supporting Information, indicates a region for firefly luciferase targeting), a sequence complementary to the primer ssDNA sequence (blue color in Figure S1 indicates two hybridization regions with primer ssDNA), and a linker sequence (black color in Figure S1). The primer ssDNA contains two hybridization regions with linear ssDNA (one portion with 16 bases at the 5′ end and another portion with 6 bases at the 3′ end).

Preparation of Circular DNA Template. Phosphorylated linear ssDNA (91 bases, 500 nM) containing two complementary sequence regions with a primer ssDNA strand (22 bases) was annealed to form circular DNA template. Two ssDNA strands were hybridized with an equal molar ratio by heating at 95 °C for 2 min and cooling down to 24 °C gradually over 1 h. The nick between the circular DNA was chemically connected by T4 DNA ligase (1 unit/μL) in the ligase buffer (30 mM Tris-HCl, pH 7.8, 10 mM $MgCl_2$, 10 mM DTT, 1 mM ATP) followed by the incubation at 24 °C for 4 h.

Synthesis of Antisense DNA Microsponge. To construct antisense DNA microsponge (ODN-MS), circular DNAs (300 nM) were mixed with ϕ29 DNA polymerase (5 units/μL) and deoxyribonucleotide triphosphate (2 mM) in the reaction buffer (40 mM Tris-HCl (pH 7.5), 50 mM KCl, 10 mM $MgCl_2$, 5 mM $(NH4)_2SO_4$, and 4 mM dithiothreitol), and then allowed to proceed at 24 °C for 24 h for the RCA process. To synthesize the fluorescently modified ODN-MS, Cyanine 5-UTP was additionally added to final concentration of 0.5 mM during the RCA reaction. For the polymeric ODN staining in ODN-MS, ssDNA-specific dye (SYBR II) was used after particle generation by following the manufacturer's instruction. The resultant product was sonicated and pipetted multiple times until the particle products were well dispersed. The solution was then centrifuged at 8000 rpm for 5 min to collect the ODN-MS product. DNase-free water was used for additional washing steps to eliminate the reagents of RCA.

Gel Electrophoresis. The molecular weight of polymeric DNAs and the stability of polymeric DNAs were characterized by gel electrophoresis. Agarose and TB buffer were mixed to a specific percent (0.5−2%) according to a weight of agarose/volume of buffer ratio (wt/vol). Mixture was heated in microwave for 1 min and then GelRed gel stain was added. The solution was immediately poured into rack and allowed to solidify for 20 min. The solidified gel in rack was transferred to gel running apparatus that was filled with TB buffer. DNA samples were prepared with a bromophenol blue containing gel loading dye by following the manufacturer's protocol (New England Biolabs, Ipswich, MA) and then loaded into gel. Gel electrophoresis was conducted at 70 (V/cm) for 60−80 (min). Gel images were visualized using UV transilluminator (Bio-Rad, Hercules, CA).

Measurement of the Polymeric DNA Concentration. Polymeric DNA structures were prepared by the addition of EDTA (50 mM), a strong Mg^{2+} scavenger, because of the disruption of polymeric DNA/inorganic composite structures of ODN-MS. The concentration of polymeric ssDNA and short ssDNA (ODN control) were measured according to manufacturer's instructions for Quant-iT OliGreen ssDNA Assay Kit (Life Technologies, Carlsbad, CA). Briefly polymeric DNA or standard solution (10 μL) were mixed well with Quant-iT OliGreen ssDNA reagent (190 μL) by pipetting. Then the mixtures were placed into a Corning Clear Flat Bottom 96-wells plate and incubated for 5 min at 24 °C. Fluorescence (λ_{ex} = 480 nm, λ_{em} = 520 nm) was measured using a fluorescence microplate reader (Tecan Infinite 200 PRO). The concentration of polymeric DNAs was determined by comparing with an ODN standard curve of fluorescence intensity *versus* concentration.

Stability Experiments of Polymeric DNA Structures. The DNA stability in serum and enzyme was analyzed by measuring the band intensities of each polymeric DNA/short DNA band in agarose gel electrophoresis. To perform serum stability test, 150 ng of polymeric DNA structures and short DNAs were incubated with 50% human serum for 3 days, 2 days, 1 day, 12 h, and 3 h. Samples were loaded into 2% agarose gel along with untreated samples of 50, 100, and 150 ng amounts as reference. Gel electrophoresis was performed at 70 V for 60 min. To perform DNase stability test, 150 ng polymeric DNA structures and short DNAs were incubated with DNase (3 units/μL) and reaction buffer. Samples were incubated for 3 days, 2 days, 1 day, 12 h, 3 h, 2 h, 90 min, 60 min, and 30 min. Samples were loaded into 2% gel along with untreated samples of 50, 100, and 150 ng amounts as reference. Gel electrophoresis was conducted at 70 V for 60 min. ImageJ densiometry analysis was processed to calculate the degradation amount (wt %) of polymeric DNA/short ssDNA.

To perform *in vivo* pharmacokinetics study, Cy5 dye-labeled polymeric ssDNA and short ssDNA were prepared. Female NCr nude mice were treated with Cy5 dye-labeled polymeric ssDNA or Cy5 labeled short ssDNA. Fluorescence intensity (λ_{ex} = 640 nm, λ_{em} = 700 nm) of dye-labeled DNA was measured from *in vivo* imaging systems (Xenogen IVIS Imaging System 200, Caliper Life Sciences, Hopkinton, MA).

Characterization of ODN-MSs and LbL-ODN-NPs. Scanning electron microscopy (JEOL JSM-6700F, JSM-6070, and JSM-6060) was utilized to obtain high-resolution digital images of the ODN-MSs, condensed nanoparticles, and LbL-ODN-NPs. Samples were prepared by placing aqueous suspensions onto silicon wafers. Images were acquired without an additional metal coating at an accelerating voltage of 2 kV.

Transmission electron microscopy (JEOL 2010 and 2000FX) was utilized to observe the internal structure of the ODN-MSs and LbL-ODN-NPs. Images were obtained at an accelerating voltage of 200 kV.

Fluorescent microscopy (Zeiss AxioSkop 2 MAT) and confocal microscopy (Nikon 1AR Spectral Scanning Confocal Microscope) were used to confirm the presence of polymeric ssDNA product in the ODN-MSs generated by the RCA. After particles formation through RCA, the ODN-MSs were stained with the ssDNA-specific dye (SYBR II) by following the company's instruction (Lonza, Walkersville, MD). Green-fluorescently stained ODN-MSs were then observed by fluorescent microscopy. Another DNA visualization method was used by adding fluorescently labeled deoxyribonucleotide (Cyanine 5-dUTP or Fluorescein) during RCA process. Confocal microscopy was then utilized to visualize the localization of DNA within microsponges. The progression of condensation was also monitored by confocal microscopy. To prepare dual-labeled fluorescence system for this observation, Fluorescein-12-dUTP (corresponding to green color) was used to construct dye-labeled ODN-MSs during RCA synthesis. Cyanine 5.5 (corresponding to red color) conjugated poly-L-lysine (PLL) (M_w 25000 g/mol) was prepared by following the previously published protocols.[45] The progression from microsponge to

polyelectrolyte complexation was observed *via* confocal microscopy at varied concentrations of dye-PLL.

The elemental composition of the ODN-MS microstructures and the condensed nanoparticles were investigated in detail using scanning transmission electron microscopy (JEOL 2010F) equipped with an analytical scanning imaging device (ASID) and an INCA energy dispersive X-ray spectroscopy (EDX) detector. Elemental mapping was carried out using a 1 nm probe.

Powder X-ray diffraction (PXRD) was used to analyze the crystalline structure of ODN-MSs and condensed nanoparticles. Samples for PXRD were prepared by placing aqueous suspensions onto copper (Cu) tapes. Data collection proceeds were achieved using a Rigaku rotating anode X-ray powder diffractometers. PXRD patterns were recorded from 5 to 40° 2Θ in a parallel beam configuration fitted with a 9 kW rotating anode copper source.

Condensation and Layer-by-Layer Assembly on ODN-MS. The condensation process of ODN-MS is properly applied to improve the delivery efficiency of polymeric DNA. The cationic polymers including PLL or PEI can be used as polymeric condensing agents by means of strong ionic interactions with negatively charged ODN-MS. To find out the optimal conditions for condensation, the polymer stock solution (*e.g.*, PLL, M_w 25000 g/mol, 5.0 mg/mL) was added into the ODN-MS solution at varied concentrations (0.1−5 mg/mL). Then the mixtures were gently mixed for 4 h. Access amount of free polymer in the supernatant was discarded by following the centrifugation at 12000 rpm for 5 min. The condensed particles were then resuspended in PBS solution and repeated washing steps twice.

For assembly of the additional layering, the variety of polymer stock solution such as PEI (M_w 25000 g/mol, 5.0 mg/mL), ssDNA (M_w 8000 g/mol, 5.0 mg/mL), and PEG−PGA (M_w 13000 g/mol, 5.0 mg/mL) were prepared separately. The condensed particles were mixed with each polymer stock solution and then allowed 4 h gentle mixing. Access amount of unreacted free polymer in the supernatant was removed by following the centrifugation at 12000 rpm for 5 min. The resultant layered particles were then resuspended in PBS solution and allowed an additional washing. This layering step could be repeated until the predefined layering numbers of LbL-ODN-NPs were achieved.

Characterization of LbL-ODN-NPs. *Dynamic Light Scattering (DLS) and Zeta Potential.* The surface charge and size of ODN-MSs and LbL-ODN-NPs were measured using zeta-potential and dynamic light scattering (DLS) instruments (Malvern Nano-ZS90 zetasizer, Westborough, MA). The particles were diluted in Milli-Q water, and three measurements were performed per each sample at 24 °C.

Intracellular Uptake Study. Cellular uptake of LbL-MS-NPs and ODN-MS was examined by confocal microscopy and flow cytometry. SKOV3 cells (1×10^5 cells) in suspension media were seeded in CELLview glas bottom dish (Greiner Bio-One GmbH, Germany) per well and maintained for 24 h. The Cy5.5 fluorescently labeled LbL-ODN-NPs or ODN-MS was added in each well in the presence of DPBS (Life Technologies, Carlsbad, CA) and then incubated for 3 h at 37 or 4 °C. At the end period of incubation, cells were washed three times with PBS and fixed with 4% paraformaldehyde. For fluorescence imaging, cells were permeabilized in 0.1% Triton X100 for 10 min and stained Alexa Fluor 488-phalloidin (Invitrogen, Carlsbad, California) and nuclei were stained with DAPI (40,6-diamidino-2-phenylindole). An antifade reagent (Invitrogen, Carlsbad, California) was added according to the manufacturer's protocol. Fluorescent images of the cells were acquired using confocal microscope (Nikon 1AR Spectral Scanning Confocal Microscope, Melville, NY).

The quantity of uptake was obtained by flow cytometry. SKOV3 cells (2×10^4 cells) in suspension media were seeded in a 96-well plate and maintained for 24 h. The Cy5.5 fluorescently labeled LbL-ODN-NPs or ODN-MS (100 μg/mL) was treated in each well in the presence of DPBS (Life Technologies, Carlsbad, CA) and then incubated for various periods of times at 37 °C. The cell-associated fluorescence was determined by flow cytometer (BD LSRFortessa) equipped with a BD high throughput sampler (HTS) for the 96-well plate format and analyzed by BD FACSDiva software (BD Biosciences, Franklin Lakes, NJ).

***In Vitro* Knockdown Experiments and Cell Proliferation Assays.** SKOV3-LUC/SKOV3 cells were used in *in vitro* knockdown evaluation and cell proliferation assay. Cells were maintained in growth media consisting of Minimum Essential Media-Alpha (MEM-α), 10% fetal bovine serum (FBS), and 1% penicillin−streptomycin. Stable both firefly and renilla luciferase-overexpressing SKOV3 cells were prepared using lentivirus vectors according to the manufacturer's protocols (Cell Biolabs, San Diego, CA).

For sample preparations, the antisense strand of firefly luciferase sequences were obtained from Ambion (Austin, TX). ODN-MSs and LbL-ODN-NPs were prepared as aforementioned procedures. The samples were diluted in DPBS (Life Technologies, Carlsbad, CA) to 10 μL final volumes for each ODN amount. The amounts of ODN-MSs and LbL-ODN-NPs were normalized to the concentration of ODN loading. A single-stranded ODN control (~22 bases) with the conventional transfection reagent (*i.e.*, lipofectamine, Invitrogen, Carlsbad, CA) was used as a positive control. As suggested by the company, the 1:3 ratio (w/v) of a single-stranded ODN/lipofectamine (ODN/Lipo) was used to form liposome. SKOV3 cells (2×10^4) were seeded in each well of a 96-wells plate and maintained. After 24 h, the MEM-α media was replaced with DPBS. The cells were treated with prepared ODN samples (10 μL) of ODN-MSs, LbL-ODN-NPs, and ODN/Lipo at varied ODN amounts were treated to the cells and then gently mixed. The cells were incubated in the controlled-temperature at 37 °C with 5% CO_2 incubator for 4 h. After 4 h of transfection DPBS was replaced with MEM-α. Both knockdown and cell proliferation evaluations were carried out after 48 h additional incubation.

For firefly luciferase silencing evaluation, the luciferase assay was performed using the Dual-Glo Luciferase Assay Kit (Promega, Madison, WI) as the kit's protocol and luminescence was measured using a microplate reader (Tecan Infinite 200 PRO). Transfections were conducted in quadruplicate. The level of firefly luciferase silencing (%) from each sample was obtained by comparing the luminescence value from *Renilla luciferase*.

The cell proliferation was evaluated using CCK-8 kit (Dojindo Molecular Technologies, Rockville, MD) following the manufacturer's protocols. Briefly, CCK-8 reagent solution (10 μL) was directly added to the each well of the plate and then the plate was incubated for 1 h at 37 °C. The amount of a water-soluble formazan (a yellow-colored product) was determined by the absorbance value at 450 nm using a microplate reader (Tecan Infinite 200 PRO). The cell proliferation (%) of each sample was determined using the absorbance value of a prepared calibration curve that contains given numbers of viable cells (untreated control).

***In Vivo* Biodistribution Experiments.** Female NCr and BALB/c nude mice (4−6 weeks old, Taconic, Hudson, NY) were used for biodistribution experiments. Mice fed on the alfalfa-free special diet (AIN-93 M Maintenance Purified Diet from TestDiet) for a week before and during experimentation to reduce the body autofluorescence level. All animal care and *in vivo* experimental procedures were performed following institutionally approved protocols and regulations (MIT Department of Comparative Medicine and NIH Principles of Laboratory Animal Care).

Biodistribution of LbL-ODN-NPs clearance was investigated in BALB/c nude mice *via* intravenous administration (*e.g.*, tail vein injection). The Cy 5.5-labeled LbL-ODN-NPs suspended in PBS were administered at the ODN concentration of 1.0 mg/kg in 0.1 mL injection volume. Whole-animal fluorescence images are obtained ventrally at the preassigned time points using IVIS whole-animal imaging system with Living Image software (Xenogen, Caliper Instruments) to measure the circulation serum half-life of the control ssDNA, polymeric DNA, and LbL-ODN-NPs. Imaging and circulation data were captured using fluorescent overlay (λ_{ex} = 640 nm, λ_{em} = 700 nm) and fitted with a 2-phase decay model (PRISM) with both slow and fast half-lives presented. For blood circulation persistence analysis of LbL-ODN-NPs, the existence of particles in blood was quantified with the Licor Odyssey system by measuring percent fluorescence recovery from collected blood samples taken after IV administration.

Statistical Analysis. All data represent mean values with standard deviation (SD) from three independent measurements. Statistical analysis between different treatments was processed by a Student's *t* test. Statistical significance was assigned for $p < 0.05$ (95% confidence level).

Conflict of Interest: The authors declare no competing financial interest.

Acknowledgment. We gratefully acknowledge the funding of this work from the DoD OCRP Teal Innovator Award (Grant Number: OC120504). We thank the MIT Koch Institute Swanson Biotechnology Center, which is supported by the Koch Institute Core Grant P30-CA14051 from the NCI, for the use of facilities, and specifically the microscopy and the flow cytometry cores. This work made use of the MIT MRSEC Shared Experimental Facilities supported by the National Science Foundation under Award Number DMR-0819762. K.E.S. thanks the National Sciences and Engineering Research Council (NSERC) for a postdoctoral fellowship. E.C.D. acknowledges postdoctoral fellowship support from the NIH (Kirschstein NRSA 1F32EB017614-01). S.W.M. is thankful for a National Science Foundation Graduate Research Fellowship (NSF GRF). We thank Dr. Mohi Quadir and Dr. Jason Deng for technical support on experiments.

Supporting Information Available: Additional results, materials, methods, and DNA nanostructure design schematic and oligonucleotide sequences. This material is available free of charge *via* the Internet at http://pubs.acs.org.

REFERENCES AND NOTES

1. Lee, J. B.; Hong, J.; Bonner, D. K.; Poon, Z.; Hammond, P. T. Self-Assembled RNA Interference Microsponges for Efficient siRNA Delivery. *Nat. Mater.* **2012**, *11*, 316–322.
2. Shopsowitz, K. E.; Roh, Y. H.; Deng, Z. J.; Morton, S. W.; Hammond, P. T. RNAi-Microsponges Form through Self-Assembly of the Organic and Inorganic Products of Transcription. *Small* **2013**, 1623–1633.
3. Gleave, M. E.; Monia, B. P. Antisense Therapy for Cancer. *Nat. Rev. Cancer* **2005**, *5*, 468–479.
4. Tamm, I.; Dörken, B.; Hartmann, G. Antisense Therapy in Oncology: New Hope for an Old Idea? *Lancet* **2001**, *358*, 489–497.
5. Bennett, C. F.; Swayze, E. E. RNA Targeting Therapeutics: Molecular Mechanisms of Antisense Oligonucleotides as a Therapeutic Platform. *Annu. Rev. Pharmacol. Toxicol.* **2010**, *50*, 259–293.
6. Kole, R.; Krainer, A. R.; Altman, S. RNA Therapeutics: Beyond RNA Interference and Antisense Oligonucleotides. *Nat. Rev. Drug Discovery* **2012**, *11*, 125–140.
7. Crooke, S. T. Progress in Antisense Technology. *Annu. Rev. Med.* **2004**, *55*, 61–95.
8. Geary, R. S.; Watanabe, T. A.; Truong, L.; Freier, S.; Lesnik, E. A.; Sioufi, N. B.; Sasmor, H.; Manoharan, M.; Levin, A. A. Pharmacokinetic Properties of 2′-O-(2-Methoxyethyl)-Modified Oligonucleotide Analogs in Rats. *J. Pharmacol. Exp. Ther.* **2001**, *296*, 890–897.
9. Zellweger, T.; Miyake, H.; Cooper, S.; Chi, K.; Conklin, B. S.; Monia, B. P.; Gleave, M. E. Antitumor Activity of Antisense Clusterin Oligonucleotides Is Improved *In Vitro* and *In Vivo* by Incorporation of 2′-O-(2-Methoxy)ethyl Chemistry. *J. Pharmacol. Exp. Ther.* **2001**, *298*, 934–940.
10. Geary, R. S.; Yu, R. Z.; Watanabe, T.; Henry, S. P.; Hardee, G. E.; Chappell, A.; Matson, J.; Sasmor, H.; Cummins, L.; Levin, A. A. Pharmacokinetics of a Tumor Necrosis Factor-A Phosphorothioate 2′-(O-Methoxyethyl) Modified Antisense Oligonucleotide: Comparison Across Species. *Drug Metab. Dispos.* **2003**, *31*, 1419–1428.
11. Deleavey, G. F.; Watts, J. K.; Damha, M. J. Chemical Modification of siRNA. In *Current Protocols in Nucleic Acid Chemistry*; Wiley: New York, 2009; Chapter 16, Unit 16.3.
12. Chauhan, V. P.; Jain, R. K. Strategies for Advancing Cancer Nanomedicine. *Nat. Mater.* **2013**, *12*, 958–962.
13. Hubbell, J. A.; Langer, R. Translating Materials Design to the Clinic. *Nat. Mater.* **2013**, *12*, 963–966.
14. Luo, D.; Saltzman, W. M. Synthetic DNA Delivery Systems. *Nat. Biotechnol.* **2000**, *18*, 33–37.
15. Petros, R. A.; DeSimone, J. M. Strategies in the Design of Nanoparticles for Therapeutic Applications. *Nat. Rev. Drug Discovery* **2010**, *9*, 615–627.
16. Juliano, R.; Bauman, J.; Kang, H.; Ming, X. Biological Barriers to Therapy with Antisense and siRNA Oligonucleotides. *Mol. Pharmaceutics* **2009**, *6*, 686–695.
17. Peer, D.; Karp, J. M.; Hong, S.; Farokhzad, O. C.; Margalit, R.; Langer, R. Nanocarriers as an Emerging Platform for Cancer Therapy. *Nat. Nanotechnol.* **2007**, *2*, 751–760.
18. Wang, A. Z.; Langer, R.; Farokhzad, O. C. Nanoparticle Delivery of Cancer Drugs. *Annu. Rev. Med.* **2012**, *63* 185–198.
19. Albanese, A.; Tang, P. S.; Chan, W. C. W. The Effect of Nanoparticle Size, Shape, and Surface Chemistry on Biological Systems. *Annu. Rev. Biomed. Eng.* **2012**, *14*, 1–16.
20. Pinheiro, A. V.; Han, D.; Shih, W. M.; Yan, H. Challenges and Opportunities for Structural DNA Nanotechnology. *Nat. Nanotechnol.* **2011**, *6*, 763–772.
21. Seeman, N. C. DNA in a Material World. *Nature* **2003**, *421*, 427–431.
22. Feldkamp, U.; Niemeyer, C. M. Rational Design of DNA Nanoarchitectures. *Angew. Chem., Int. Ed. Engl.* **2006**, *45*, 1856–1876.
23. Aldaye, F. A.; Palmer, A. L.; Sleiman, H. F. Assembling Materials with DNA as the Guide. *Science* **2008**, *321*, 1795–1799.
24. Roh, Y. H.; Ruiz, R. C. H.; Peng, S.; Lee, J. B.; Luo, D. Engineering DNA-Based Functional Materials. *Chem. Soc. Rev.* **2011**, *40*, 5730–5744.
25. Wilner, O. I.; Willner, I. Functionalized DNA Nanostructures. *Chem. Rev.* **2012**, *112*, 2528–2556.
26. Bhatia, D.; Surana, S.; Chakraborty, S.; Koushika, S. P.; Krishnan, Y. A Synthetic Icosahedral DNA-Based Host-Cargo Complex for Functional *In Vivo* Imaging. *Nat. Commun.* **2011**, *2*, 339.
27. Walsh, A. S.; Yin, H.; Erben, C. M.; Wood, M. J. A.; Turberfield, A. J. DNA Cage Delivery to Mammalian Cells. *ACS Nano* **2011**, *5*, 5427–5432.
28. Keum, J.-W.; Ahn, J.-H.; Bermudez, H. Design, Assembly, and Activity of Antisense DNA Nanostructures. *Small* **2011**, *7*, 3529–3535.
29. Lee, J. B.; Roh, Y. H.; Um, S. H.; Funabashi, H.; Cheng, W.; Cha, J. J.; Kiatwuthinon, P.; Muller, D. A.; Luo, D. Multifunctional Nanoarchitectures from DNA-Based ABC Monomers. *Nat. Nanotechnol.* **2009**, *4*, 430–436.
30. Lee, H.; Lytton-Jean, A. K. R.; Chen, Y.; Love, K. T.; Park, A. I.; Karagiannis, E. D.; Sehgal, A.; Querbes, W.; Zurenko, C. S.; Jayaraman, M.; *et al.* Molecularly Self-Assembled Nucleic Acid Nanoparticles for Targeted *In Vivo* siRNA Delivery. *Nat. Nanotechnol.* **2012**, *7*, 389–393.
31. Drmanac, R.; Sparks, A. B.; Callow, M. J.; Halpern, A. L.; Burns, N. L.; Kermani, B. G.; Carnevali, P.; Nazarenko, I.; Nilsen, G. B.; Yeung, G.; *et al.* Human Genome Sequencing Using Unchained Base Reads on Self-Assembling DNA Nanoarrays. *Science* **2010**, *327*, 78–81.
32. Lee, J. B.; Peng, S.; Yang, D.; Roh, Y. H.; Funabashi, H.; Park, N.; Rice, E. J.; Chen, L.; Long, R.; Wu, M.; *et al.* A Mechanical Metamaterial Made from a DNA Hydrogel. *Nat. Nanotechnol.* **2012**, *7*, 816–820.
33. Decher, G. Fuzzy Nanoassemblies: Toward Layered Polymeric Multicomposites. *Science* **1997**, *277*, 1232–1237.
34. Krogman, K. C.; Lowery, J. L.; Zacharia, N. S.; Rutledge, G. C.; Hammond, P. T. Spraying Asymmetry into Functional Membranes Layer-by-Layer. *Nat. Mater.* **2009**, *8*, 512–518.
35. Schneider, G. F.; Subr, V.; Ulbrich, K.; Decher, G. Multifunctional Cytotoxic Stealth Nanoparticles. A Model Approach with Potential for Cancer Therapy. *Nano Lett.* **2009**, *9*, 636–642.
36. Hammond, P. T. Form and Function in Multilayer Assembly: New Applications at the Nanoscale. *Adv. Mater.* **2004**, *16*, 1271–1293.
37. Hammond, P. T. Building Biomedical Materials Layer-by-Layer. *Mater. Today* **2012**, *15*, 196–206.

38. Becker, A. L.; Johnston, A. P. R.; Caruso, F. Layer-by-Layer-Assembled Capsules and Films for Therapeutic Delivery. *Small* **2010**, *6*, 1836–1852.
39. Hammond, P. Polyelectrolyte Multilayered Nanoparticles: Using Nanolayers for Controlled and Targeted Systemic Release. *Nanomedicine* **2012**, *7*, 619–622.
40. Boudou, T.; Crouzier, T.; Ren, K.; Blin, G.; Picart, C. Multiple Functionalities of Polyelectrolyte Multilayer Films: New Biomedical Applications. *Adv. Mater.* **2010**, *22*, 441–467.
41. Elbakry, A.; Zaky, A.; Liebl, R.; Rachel, R.; Goepferich, A.; Breunig, M. Layer-by-Layer Assembled Gold Nanoparticles for siRNA Delivery. *Nano Lett.* **2009**, *9*, 2059–2064.
42. Cortez, C.; Tomaskovic-Crook, E.; Johnston, A. P. R.; Radt, B.; Cody, S. H.; Scott, A. M.; Nice, E. C.; Heath, J. K.; Caruso, F. Targeting and Uptake of Multilayered Particles to Colorectal Cancer Cells. *Adv. Mater.* **2006**, *18*, 1998–2003.
43. Poon, Z.; Lee, J. B.; Morton, S. W.; Hammond, P. T. Controlling *In Vivo* Stability and Biodistribution in Electrostatically Assembled Nanoparticles for Systemic Delivery. *Nano Lett.* **2011**, *11*, 2096–2103.
44. Poon, Z.; Chang, D.; Zhao, X.; Hammond, P. T. Layer-by-Layer Nanoparticles with a pH-Sheddable Layer for *In Vivo* Targeting of Tumor Hypoxia. *ACS Nano* **2011**, *5*, 4284–4292.
45. Morton, S. W.; Poon, Z.; Hammond, P. T. The Architecture and Biological Performance of Drug-Loaded LbL Nanoparticles. *Biomaterials* **2013**, *34*, 5328–5335.
46. Sexton, A.; Whitney, P. G.; Chong, S.-F.; Zelikin, A. N.; Johnston, A. P. R.; De Rose, R.; Brooks, A. G.; Caruso, F.; Kent, S. J. A Protective Vaccine Delivery System for *In Vivo* T Cell Stimulation Using Nanoengineered Polymer Hydrogel Capsules. *ACS Nano* **2009**, *3*, 3391–3400.
47. Shutava, T. G.; Balkundi, S. S.; Vangala, P.; Steffan, J. J.; Bigelow, R. L.; Cardelli, J. A.; O'Neal, D. P.; Lvov, Y. M. Layer-by-Layer-Coated Gelatin Nanoparticles as a Vehicle for Delivery of Natural Polyphenols. *ACS Nano* **2009**, *3*, 1877–1885.
48. Saul, J. M.; Wang, C.-H. K.; Ng, C. P.; Pun, S. H. Multilayer Nanocomplexes of Polymer and DNA Exhibit Enhanced Gene Delivery. *Adv. Mater.* **2008**, *20*, 19–25.
49. Blanco, L.; Bernad, A.; Lazaro, J.; Martin, G.; Garmendia, C.; Salas, M. Highly Efficient DNA Synthesis by the Phage Phi 29 DNA Polymerase. Symmetrical Mode of DNA Replication. *J. Biol. Chem.* **1989**, *264*, 8935–8940.
50. Luo, D. The Road from Biology to Materials. *Mater. Today* **2003**, *6*, 38–43.
51. Mok, H.; Lee, S. H.; Park, J. W.; Park, T. G. Multimeric Small Interfering Ribonucleic Acid for Highly Efficient Sequence-Specific Gene Silencing. *Nat. Mater.* **2010**, *9*, 272–278.
52. Boussif, O.; Lezoualc'h, F.; Zanta, M. A.; Mergny, M. D.; Scherman, D.; Demeneix, B.; Behr, J. P. A Versatile Vector for Gene and Oligonucleotide Transfer into Cells in Culture and *In Vivo*: Polyethylenimine. *Proc. Natl. Acad. Sci. U. S. A.* **1995**, *92*, 7297–7301.
53. Trubetskoy, V. S.; Wong, S. C.; Subbotin, V.; Budker, V. G.; Loomis, A.; Hagstrom, J. E.; Wolff, J. A. Recharging Cationic DNA Complexes with Highly Charged Polyanions for *In Vitro* and *In Vivo* Gene Delivery. *Gene Ther.* **2003**, *10*, 261–271.
54. Shchukin, D. G.; Patel, A. A.; Sukhorukov, G. B.; Lvov, Y. M. Nanoassembly of Biodegradable Microcapsules for DNA Encasing. *J. Am. Chem. Soc.* **2004**, *126*, 3374–3375.
55. Harris, J. M.; Chess, R. B. Effect of Pegylation on Pharmaceuticals. *Nat. Rev. Drug Discovery* **2003**, *2*, 214–221.
56. Geary, R. S.; Watanabe, T. A.; Truong, L.; Freier, S.; Lesnik, E. A.; Sioufi, N. B.; Sasmor, H.; Manoharan, M.; Levin, A. A. Pharmacokinetic Properties of 2′-O-(2-Methoxyethyl)-Modified Oligonucleotide Analogs in Rats. *J. Pharmacol. Exp. Ther.* **2001**, *296*, 890–897.
57. Harrington, K. J.; Rowlinson-Busza, G.; Syrigos, K. N.; Uster, P. S.; Abra, R. M.; Stewart, J. S. Biodistribution and Pharmacokinetics of 111In-DTPA-Labelled Pegylated Liposomes in a Human Tumour Xenograft Model: Implications for Novel Targeting Strategies. *Br. J. Cancer* **2000**, *83*, 232–238.
58. Morton, S. W.; Shah, N. J.; Quadir, M. A.; Deng, Z. J.; Poon, Z.; Hammond, P. T. Osteotropic Therapy *via* Targeted Layer-by-Layer Nanoparticles. *Adv. Healthcare Mater.* **2014**, *3*, 867–875.
59. Deng, Z. J.; Morton, S. W.; Ben-Akiva, E.; Dreaden, E. C.; Shopsowitz, K. E.; Hammond, P. T. Layer-by-Layer Nanoparticles for Systemic Codelivery of an Anticancer Drug and siRNA for Potential Triple-Negative Breast Cancer Treatment. *ACS Nano* **2013**, *7*, 9571–9584.